Applied Surface Science 440 (2018) 153–161

Contents lists available at ScienceDirect

Applied Surface Science

journal homepage: www.elsevier.com/locate/apsusc

Full Length Article

Novel microwave-assisted synthesis of porous g-C_3N_4/SnO_2 nanocomposite for solar water-splitting

A. Seza [a], F. Soleimani [a], N. Naseri [b], M. Soltaninejad [a], S.M. Montazeri [a], S.K. Sadrnezhaad [a,*], M.R. Mohammadi [a], H. Asgari Moghadam [a], M. Forouzandeh [b], M.H. Amin [c]

[a] Department of Materials Science and Engineering, Sharif University of Technology, Azadi Ave., P.O. Box: 11155-9466, Tehran, Iran
[b] Department of Physics, Sharif University of Technology, Azadi Ave., P.O. Box 11155-9161, Tehran, Iran
[c] Centre for Advanced Materials and Industrial Chemistry, School of Sciences, RMIT Universit, Melbourne, VIC 3001, Australia

ARTICLE INFO

Article history:
Received 17 August 2017
Revised 23 December 2017
Accepted 14 January 2018

Keywords:
g-C_3N_4/SnO_2 nanocomposite
Carbon nitride
Microwave
Porous
Visible light catalyst
Water-splitting

ABSTRACT

Highly porous nanocomposites of graphitic-carbon nitride and tin oxide (g-C_3N_4/SnO_2) were prepared through simple pyrolysis of urea molecules under microwave irradiation. The initial amount of tin was varied in order to investigate the effect of SnO_2 content on preparation and properties of the composites. The synthesized nanocomposites were well-characterized by XRD, FE-SEM, HR-TEM, BET, FTIR, XPS, DRS, and PL. A homogeneous distribution of SnO_2 nanoparticles with the size of less than 10 nm on the porous C_3N_4 sheets could be obtained, suggesting that in-situ synthesis of SnO_2 nanoparticles was responsible for the formation of g-C_3N_4. The process likely occurred by the aid of the large amounts of OH groups formed on the surfaces of SnO_2 nanoparticles during the polycondensation reactions of tin derivatives which could facilitate the pyrolysis of urea to carbon nitride. The porous nanocomposite prepared with initial tin amount of 0.175 g had high specific surface area of 195 $m^2 g^{-1}$ which showed high efficiency photo-electrochemical water-splitting ability. A maximum photocurrent density of 33 μA cm^{-2} was achieved at an applied potential of 0.5 V when testing this nanocomposite as photo-anode in water-splitting reactions under simulated visible light irradiation, introducing it as a promising visible light photoactive material.

1. Introduction

Over the past years, numerous studies have been conducted on photocatalyst materials and their applications such as environmental protection and energy production [1]. Photocatalytic hydrogen production is one of the futuristic procedures in order to generate hydrogen as a renewable green energy source alternative to polluting fossil fuels [2]. During the Photoelectrochemical (PEC) water-splitting, solar energy can aid the hydrogen production reactions to occur at an electrode coated by specific semiconductors or photocatalyst materials [2,3].

Despite the fact that many of these materials have shown promising photocatalytic behavior under irradiation of ultraviolet (UV) light, reaching a high-performance material with efficient activity in the visible light range is still a challenge [4]. This could be achieved by developing materials with engineered band-gaps in which potential enhancement in charge transfer and electron-hole separation leads to enhanced visible light photocatalytic activity [5]. As an approach, coupling semiconductors with proper energy band positions can lead to the formation of heterojunction structures with enhanced charge separation ability [4].

Graphitic carbon nitride (g-C_3N_4) with the band-gap energy of around 2.7 eV is a promising material with various applications such as photocatalytic water-splitting, pollutant removal, and biotechnology [6,7]. It is a two-dimensional polymer build up by either s-triazine (C_3N_3) based units or tri-s-triazine (heptazine) structures with van der Waals interactions between the polymeric layers [8]. The g-C_3N_4 can be synthesized using various precursors, such as cyanamide, melamine, and urea [9]. Among them, urea is a low-cost, abundant, and nontoxic compound which can be simply pyrolyzed to form g-C_3N_4 [10,11]. Thermal polymerization of urea to g-C_3N_4 is one of the efficient methods for preparing high-performance, cost-effective g-C_3N_4, and its composites. Nonetheless, some drawbacks are still challenging. For instance, the simple pyrolysis of urea by means of thermal energy (e.g. heating urea mainly at 550 °C for several hours) will not yield carbon nitride efficiently [9,12]. so other methods like microwave-assisted synthesis should be considered [13].

* Corresponding author.
E-mail address: sadrnezh@sharif.edu (S.K. Sadrnezhaad).

https://doi.org/10.1016/j.apsusc.2018.01.133
0169-4332/

In order to promote g-C_3N_4 applications, various modifications can be conducted such as adding different particles or materials on the surfaces of the graphitic sheets or into the porous layers of g-C_3N_4. These procedures can increase the electron-hole separation time; leading to the enhanced photocatalytic activity of g-C_3N_4, as mentioned above for the case of semiconductors coupling [12,14]. Tin oxide (SnO_2) with the band gap energy of around 3.6 eV is one of such materials which can provide unique outcomes in contact with g-C_3N_4. According to the previous researches [15–19], incorporation of SnO_2 nanoparticles into the carbon nitride sheets can result in the formation of nanocomposites with enhanced visible-light photocatalytic behavior.

Here we introduced a novel, cost-effective microwave-assisted method for synthesis of highly porous g-C_3N_4/SnO_2 nanocomposites by using urea as a precursor of g-C_3N_4 and dissolving tin in hydrochloric acid for preparing tin chloride solution. The reason for not using tin chloride straightly was that the whole synthesis procedure can be linked to a hydrometallurgical leaching process for recovery of tin from various sources of metal wastes such as electronic waste. This is for the first time, to the best of the authors' knowledge, that urea is pyrolyzed under the microwave irradiation in a solution containing tin ions. The resulted g-C_3N_4/SnO_2 nanocomposites were well-characterized and their ability for photoelectrochemical water-splitting under simulated visible light was investigated.

2. Materials and methods

2.1. Synthesis of g-C_3N_4/SnO_2 nanocomposites

Urea (Merck) as the precursor of carbon nitride and commercially available pure tin were used without any modification. An analytical grade of hydrochloric acid (HCl) 37% (density of 1.19 g cm^{-3}) and ammonium hydroxide 25% were supplied by Merck. Ethanol and de-ionized (DI) water were purchased from a local chemical supplier. The g-C_3N_4/SnO_2 nanocomposite was synthesized following the procedure described below.

A proper amount of tin was dissolved in 10 ml Hydrochloric acid for three hours. 300 ml of ammonium hydroxide solution was added to the above mixture in order to adjust the pH to a basic value of 12. Then, 1.5 g urea was added to the solution with further homogenization. The beaker was placed in a microwave oven operated at 2.45 GHz and 900 W for 30 min. a pipe venting system was installed through the roof of microwave oven for removing the gases products from the synthesis environment. The final product was washed with DI-water and ethanol and after centrifuging for 5 min at 4000 rpm, it was placed in an oven at 180 °C for 48 h and kept in dark before subsequent analyses. Samples were named according to the amount of tin used as S-X, where X refers to the initial weight of tin which was 0.175, 0.6, and 1 g. In order to compare the results with traditional methods, g-C_3N_4 was prepared by heating melamine at 550 °C for 3 h at a crucible. Pristine SnO_2 nanoparticles were also prepared through heating of the S-0.175 composite at 600 °C for about four hours, the procedure in which decomposition of carbon nitride would occur.

2.2. Characterizations

X-ray Diffraction (XRD) patterns of the pure materials and the obtained nanocomposites were recorded using a Philips X'Pert Pro MPD with a Cu-K_α radiation source. Investigation of the morphology of the nanocomposites and the dimensions of C_3N_4 sheets was carried out using a field-emission scanning electron microscope (FESEM, Tescan Mira 3-XMU). High-resolution transmission electron microscopy (HR-TEM) studies were carried out on a JEM-2100F device equipped with a Gatan Orius SC1000 CCD camera and the accelerating voltage was 80 kV. The sample was sonicated in acetone for approximately 10 min by further deposition of a few drops on a carbon-coated copper grid. EDS mapping was prepared in Scanning-TEM mode using an Oxford XMax-80T EDS detector. The specific surface area of the samples was calculated by the Brunauer-Emmett-Teller (BET) method (NanoSORD, Iran) through N_2 adsorption/desorption. Fourier-transformed infrared (FTIR) spectra were recorded by a Nexus 470 (Nicolet, Germany). All samples were dried before the test, grounded with KBr and pressed into a pellet. X-ray photoelectron spectroscopy (XPS) was performed using a Thermo K-alpha XPS equipped with an Al-K_α radiation (1486.6 eV) X-ray source. A survey scan was conducted using a pass energy of 200 eV to determine possible contaminants. The photoluminescence (PL) spectra of the samples were measured with a a Varian Cary Eclipse at excitation wavelength of 280 nm at room temperature. The UV–vis diffuse reflectance spectra (DRS) of the samples were recorded on an AvaSpec 2048 TEC spectrometer.

2.3. PEC Analysis

Electrochemical analyses were conducted on the electrodes prepared from the fabricated powders. In this regard, the synthesized powders were first converted into a paste and then deposited on a fluorine-doped tin oxide (FTO) substrate. The pastes were prepared by mixing the synthesized powders, a solvent and a binder as reported elsewhere [20]. All photo-electrochemical measurements were performed in 0.2 M Na_2SO_4 solution in a glassy reactor equipped with a quartz window for illuminating the sample. Photocurrents were recorded using a three-electrode work station (OrigaFlex-OGF01) with the paste samples, Ag/AgCl, and Pt rod as working, reference, and counter electrodes, respectively. The light source was Xe lamp with solar-like spectrum in which thermal radiation was eliminated using IR filter.

2.4. Methylene blue (MB) degradation

28 mg of each powder was dispersed in 50 mL DI-water via 5 min sonication. Then, a proper amount of MB aqueous solution (1 mM) as a model dye was added to each sample to reach initial dye concentration of 5.5 mg L^{-1}. The mixtures were magnetically stirred in the dark for 30 min to reach the adsorption-desorption equilibrium. Samples were visible-light irradiated for 3 h while stirred. The light source was a 400 W Hg vapor lamp with a 400 nm cut-off filter. After irradiation, samples were centrifuged and the concentration of MB was determined by measuring the absorbance at ~660 nm using a UV–Vis spectrophotometer.

3. Results and discussion

According to the previous researches, the content of SnO_2 in g-C_3N_4/SnO_2 composites could be simply calculated from the weight of the residuals after heating the samples to 800 °C [21,22]. Following the same approach in the present study, the g-C_3N_4 mass ratios are obtained as 12.3%, 4.4%, and 1.9% for the samples S-0.175, S-0.6, and S-1, respectively. It should be noted that our method of synthesis was unsuccessful when the initial amount of tin was less than 0.175 g. So, the higher contents of g-C_3N_4 could not be reached. This will be more discussed in the following paragraphs.

Fig. 1 represents the XRD patterns of pure g-C_3N_4, pristine SnO_2 nanoparticles, and their composites prepared by the microwave-assisted method. According to the figure, pure g-C_3N_4 shows a characteristic peak at $2\theta = 27.3°$ which corresponds to (0 0 2) reflection of the stacked sheets [23]. For tin oxide nanoparticles with tetragonal structure, the peaks at 2θ of 26.6°, 33.5°,51.5°,

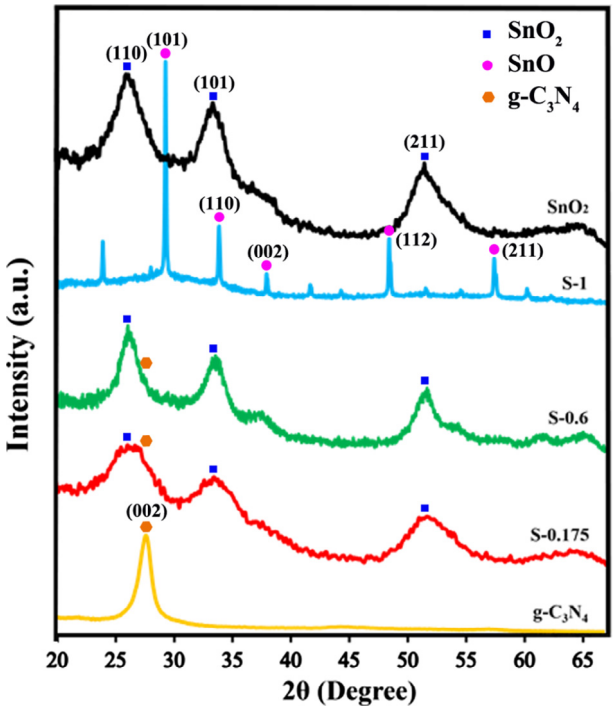

Fig. 1. X-ray diffraction patterns of SnO_2 nanoparticles, pure g-C_3N_4, and their composites synthesized with the various initial weight of Sn.

and 65.1° are expected, as can be seen in the relevant XRD pattern and these reflections are also observed in the XRD pattern of S-0.175 and S-0.6 samples. However, asymmetric shape of the first peak could be attributed to the overlapping of two characteristic peaks of SnO_2 (1 1 0) and C_3N_4 (0 0 2) reflections [17,19]. A quite different pattern is obtained for the sample S-1, which is likely attributed to the formation of the rather stable compounds of SnO_x, mostly with x = 1 [24,25]. The absence of SnO_2 nanoparticles can be responsible for the lack of the formation of g-C_3N_4.

According to Scherrer equation, $D = k\,\lambda/(B\cos\theta)$, mean crystallite size for the tin oxide nanoparticles in the pure form and in the nanocomposite samples was calculated. In this equation, D represents particles diameter, k is a constant (0.9), λ stands for X-ray wavelength (0.1541 nm), B represents the Full-Width at Half Maximum (FWHM, in radians), and θ is the angle of the diffracted peak in degrees [26]. Two peaks of SnO_2 (1 0 1) and (2 1 1) reflections were considered in the measurements and the average results were around 6.8, 10.3, and 7.0 nm for the samples S-0.175, S-0.6, and pure SnO_2, respectively. Increasing the initial amount of tin results in the formation of larger SnO_2 particles and concurrently decreases the g-C_3N_4 content. It is concluded that the synthesis of ultra-small SnO_2 particles is a prerequisite for the formation of carbon nitride sheets.

Fig. 2 represents the morphology of the S-0.175 nanocomposite through FE-SEM analysis. Large-scale stacked layers of graphitic carbon nitride can be observed in Fig. 2a. Additionally, Fig. 2b shows the highly porous structure of the carbon nitride sheets. According to this image, several pores exist on the surface of the graphitic layers and the layers are damaged in some areas. The direct microwave irradiation and exothermic decomposition of urea are probably responsible for this phenomenon. Closer SEM view of the nanocomposite indicates the presence of both SnO_2 nanoparticles and sub-micron sized pores on the carbon nitride sheets (Fig. 2c). It is shown that the depth of the pores is not in the same size on different regions of the layers, suggesting that several layers in the graphitic stacks can be affected by microwave radiations through the same direction. These pores are surrounded by SnO_2 nanoparticles aggregates which indicates the high affinity of these particles to accumulate on the large surfaces of carbon nitride layers.

The high-resolution TEM images of this sample are shown in Fig. 3. According to Fig. 3a, aggregates of tin oxide nanoparticles are clearly seen on a carbon nitride sheet. Fig. 3b reveals a porous structure of the graphitic C_3N_4 in the as-prepared nanocomposite while SnO_2 nanoparticles surround these pores as mentioned before. The high level of porosity of this nanocomposite is further evidenced by calculation of the specific surface area through BET analysis (S_{BET}), which is about 195 $m^2\ g^{-1}$. The values of S_{BET} are about 17 and 101 $m^2\ g^{-1}$ for g-C_3N_4 and pure SnO_2 samples, respectively. The formation of gaseous products such as NH_3 and CO_2 can be responsible for the observed highly porous sheets [27] which are discussed below.

During the irradiation of microwave, some of the urea molecules possibly undergo complete thermal decomposition to gaseous products rather than the process of condensation and pyrolysis. These molecules can be located between the graphitic layers of C_3N_4 by either diffusion or intercalation into the layers. In the case of intercalated molecules, further irradiation of microwave can cause the exothermic decomposition of urea to some extents. So, gaseous products would be formed and confined thereafter between the graphitic layers of C_3N_4. The tendency of such gases to escape from the layers can cause interconnected porosities on the graphitic sheets. It should be mentioned that since the synthesis procedure was conducted in an ammonia solution medium,

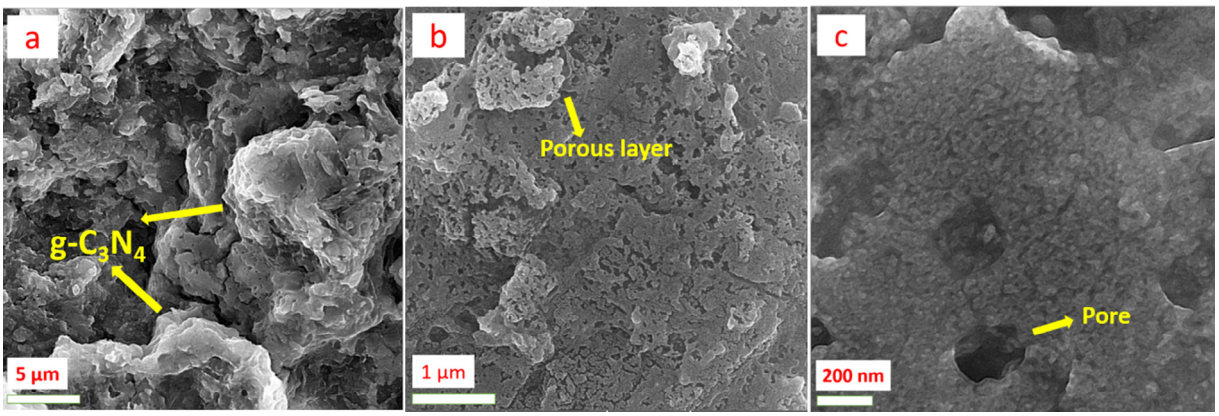

Fig. 2. FE-SEM micrographs of S-0.175 nanocomposite prepared by microwave irradiation: (a) stacked layers of graphitic carbon nitride; (b) porous structure of the carbon nitride layers; (c) aggregates of tin oxide nanoparticles on the sheets of carbon nitride at the vicinity of the pores.

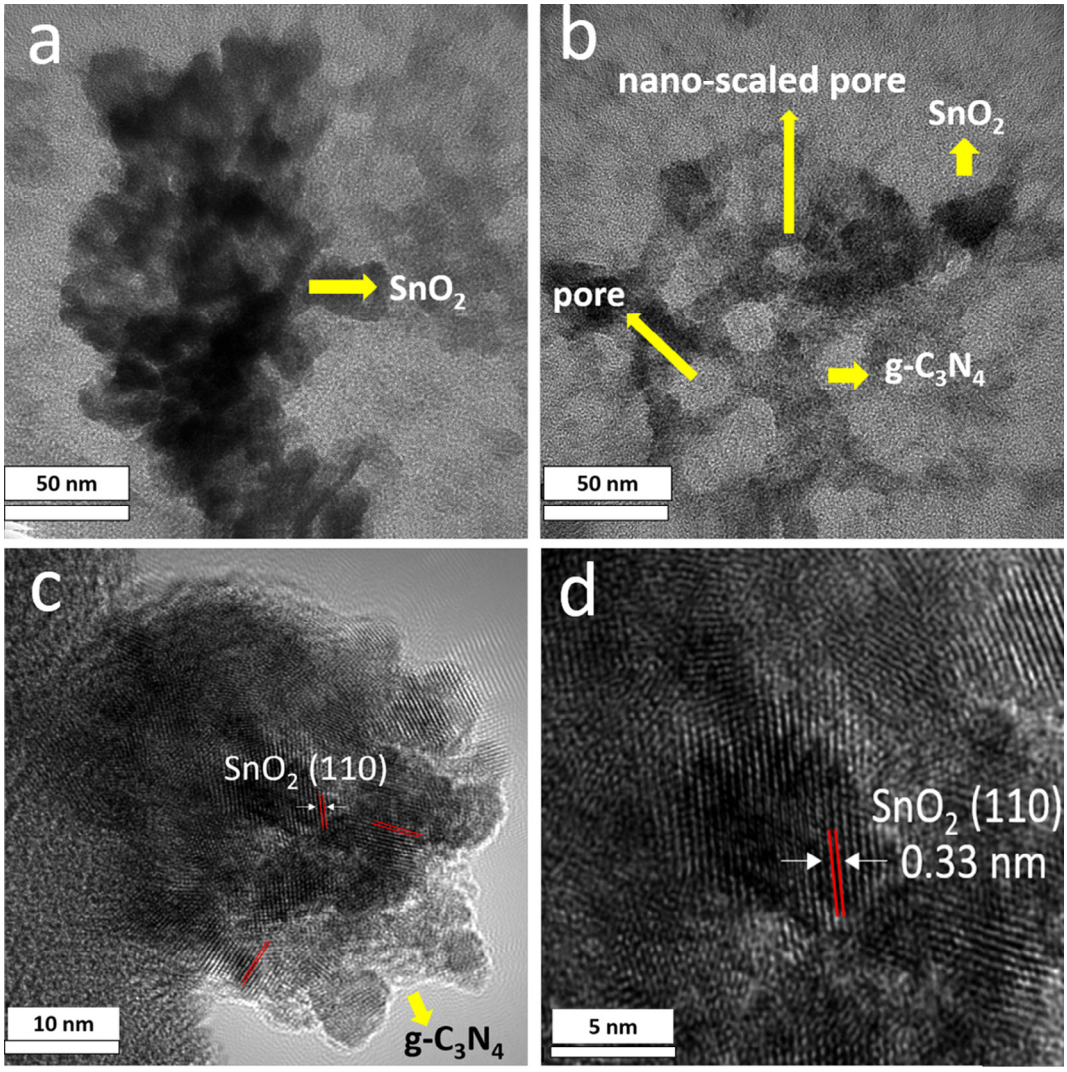

Fig. 3. HR-TEM image of S-0.175: (a) aggregates of SnO_2 nanoparticles on a sheet of C_3N_4; (b) porous structure of C_3N_4 layers with the SnO_2 nanoparticles surrounding the pores; (c) nanoparticles arrangements on a C_3N_4 sheet; (d) lattice distance of SnO_2 nanoparticles.

similar thermal combustion process can occur for the ammonia molecules.

Fig. 3c and d shows lattice arrangements of the nanoparticles attached to the carbon nitride sheets. The lattice distance that equals to 0.33 nm is indexed to the (1 1 0) planes of the tetragonal structure of SnO_2 particles located on a carbon nitride sheet. The average diameter of these nanoparticles is measured to be about 7.0 nm, which shows good agreement with the crystallite size calculated by the Scherrer equation. It is deduced that gases produced from the decomposition of ammonia and/or urea can act as inhibitors against particles growth. Since the nanoparticles are dispersed by colliding with the existing gases, their growth mechanisms are hindered by a large amount of gaseous products [28]. Fig. 3d shows the lattice arrangements in higher magnification which indicates the contact between the g-C_3N_4 and SnO_2 nanoparticles that can result in heterojunction structure and appropriate charge transfer [29].

Fig. 4 represents the element mapping images of the S-0.175 sample. According to the image, the existence of the carbon, nitrogen, tin, and oxygen can be inferred. The homogeneous presence of the tin and oxygen alongside the carbon and nitrogen elements throughout the grid indicates the uniform distribution of the SnO_2 nanoparticles on the carbon nitride sheets. The overlap of the four elements can show the coupling of the SnO_2 nanoparticles with g-C_3N_4 layers [29].

The interactions between SnO_2 and carbon nitride sheets can be further investigated through the comparison of FTIR spectra for pure g-C_3N_4, pristine SnO_2 nanoparticles, and their nanocomposite (Fig. 5). The spectrum of pure C_3N_4 shows a peak at around 808 cm^{-1} which can be assigned to tri-s-Triazine or heptazine units, and a series of vibrational peaks between 1100 cm^{-1} and 1660 cm^{-1} which corresponds to the stretching mode of C—N heterocycles. Pure SnO_2 shows a band at around 529 cm^{-1} which correspond to Sn—O stretching vibration. This band is also observed in the spectrum of S-0.175 in addition to the vibrations of C—N heterocycles. The peak assigned to tri-s-Triazine is shifted to 780 cm^{-1}, indicating that the corresponding binding energy is lowered due to the attachment of SnO_2 to C_3N_4. Moreover, the peak at around 2819 cm^{-1} can be attributed to —CH_x groups and the broad vibrational band between 3000 and 3500 cm^{-1} is ascribed to – NH and hydroxyl (—OH) functional groups, suggesting that SnO_2 nanoparticles are more likely to attach to the C_3N_4 sheets *via* hydrogen bonds [26]. However, the presence of a weak band at 1074 cm^{-1} can be correlated to the formation of Sn—O—C bonds to some extents.

For investigating the elemental chemical states and chemical composition of the S-0.175 nanocomposite, the high-resolution X-ray photoelectron spectrums of C 1s, N 1s, O 1s, and Sn 3d are presented in Fig. 6. The deconvolution of the C 1s signal (Fig. 6a)

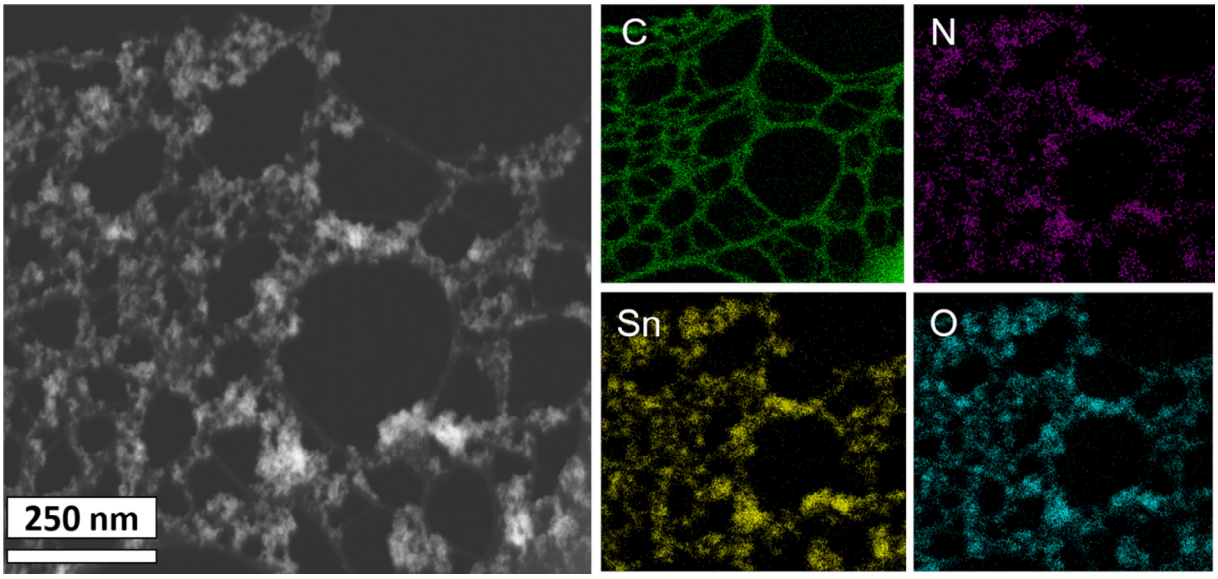

Fig. 4. Elemental mapping based on energy dispersive spectroscopy (EDS) of the g-C_3N_4/SnO_2 nanocomposite.

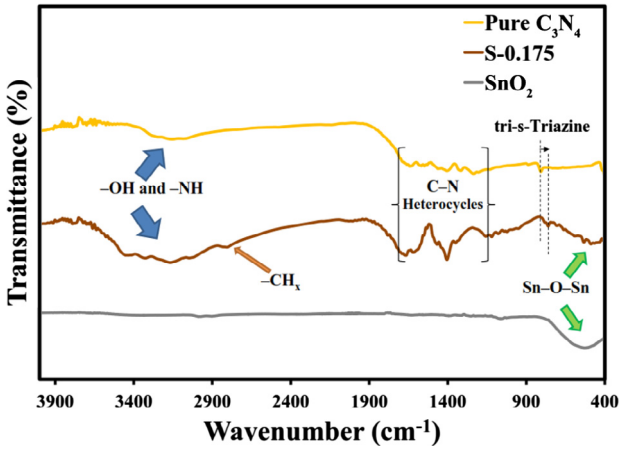

Fig. 5. Fourier-transformed infrared spectroscopy (FTIR) of the g-C_3N_4, SnO_2, and their nanocomposite with the initial tin amount of 0.175 g.

indicates three contributions for carbon atoms: the peak at 284.8 eV corresponds to the adventitious carbon, the binding energy of 286.5 eV can be indexed to the tertiary carbon C—$(N)_3$ groups, and the sp^2-hybridized carbon atoms in the aromatic ring (N—C=N coordination) are identified by the peak at 289.5 eV.

Fig. 6b represents the deconvolution of the N 1s signal with three major contributions. In this spectrum, the large peak at a binding energy of 400.5 eV is attributed to the pyridine-like structure of the s-triazine unit (C—N=C). The peak at a binding energy of 401.1 eV is ascribed to the nitrogen atom binding with three carbon atoms ($N—(C)_3$ groups) at the center of heptazine rings. The peak at 402.5 eV corresponds to the presence of N—H groups which is in a good agreement with FTIR spectrum of the nanocomposite sample.

The presence of SnO_2 in the nanocomposite is surveyed by considering Sn 3d signal in Fig. 6c. Two peaks at binding energies of 487.5 and 495.9 eV can be assigned to the Sn $3d_{3/2}$ and Sn $3d_{5/2}$, respectively. The XPS spectrum of O 1 s (Fig. 6d) shows the main contribution at 532.2 eV that corresponds to the SnO_2 nanoparticles. By comparing with pure SnO_2 XPS data, a slight shift in binding energy towards lower energies is observed for both oxygen and tin spectra which can be attributed to the interactions between SnO_2 nanoparticles and carbon nitride layers [30].

Fig. 7 schematically shows a mechanism which likely occurs during the synthesis procedure. To begin with, the above experiments were conducted while the tin precursors were removed from the solution and it was inferred that carbon nitride could not be synthesized *via* the microwave-assisted method. In other words, tin derivatives are responsible for carbon nitride preparation from urea in the solution. This hypothesis can be further interpreted according to the study of Zou et al. [31]. In their research, carbon nitride has been directly synthesized from urea over the OH-rich mesoporous TiO_2 spheres, and the OH groups bonded to the TiO_2 spheres with large surface areas have been responsible for the conversion of urea derivatives to the carbon nitride. In the present study, by the addition of ammonia to the aqueous tin chloride as the starting solution, tin hydroxide was prepared and subsequent irradiation of microwave could lead to condensation process and synthesis of ultra-small SnO_2 nanoparticles with the presence of surface OH groups coming from connecting the metal centers with Sn-OH-Sn bridges [32]. Further microwave heating might result in the decomposition of urea to isocyanic acid that could act as a building precursor of heptazine unit by converting to the cyanamide. This process was conducted with the aid of SnO_2 nanoparticles acting as catalysts.

From the viewpoint of the urea molecules, they can make their influence in two ways during the synthesis process. Firstly, gases produced from urea decomposition can hinder nanoparticles growth. In the second, urea molecule decomposition to isocyanic acid can lead to the formation of carbon nitride with the aid of nanoparticle surfaces and the establishment of hydrogen bonds through OH-rich surfaces.

Investigation of the optical properties of the nanocomposites is conducted by UV–vis diffuse reflectance spectroscopy. According to the obtained Tauc plots of the samples (Fig. 8), band gap energies (E_g) of the synthesized nanocomposites are located between the band gap energy of pure g-C_3N_4 and SnO_2 which are 2.7 and 3.53, respectively. However, the band gap energy is shifted towards the band gap energy of 3 eV as SnO_2 content increases, representing the presence of tin oxide nanoparticles on the carbon nitride layers after being synthesized via the microwave-assisted method.

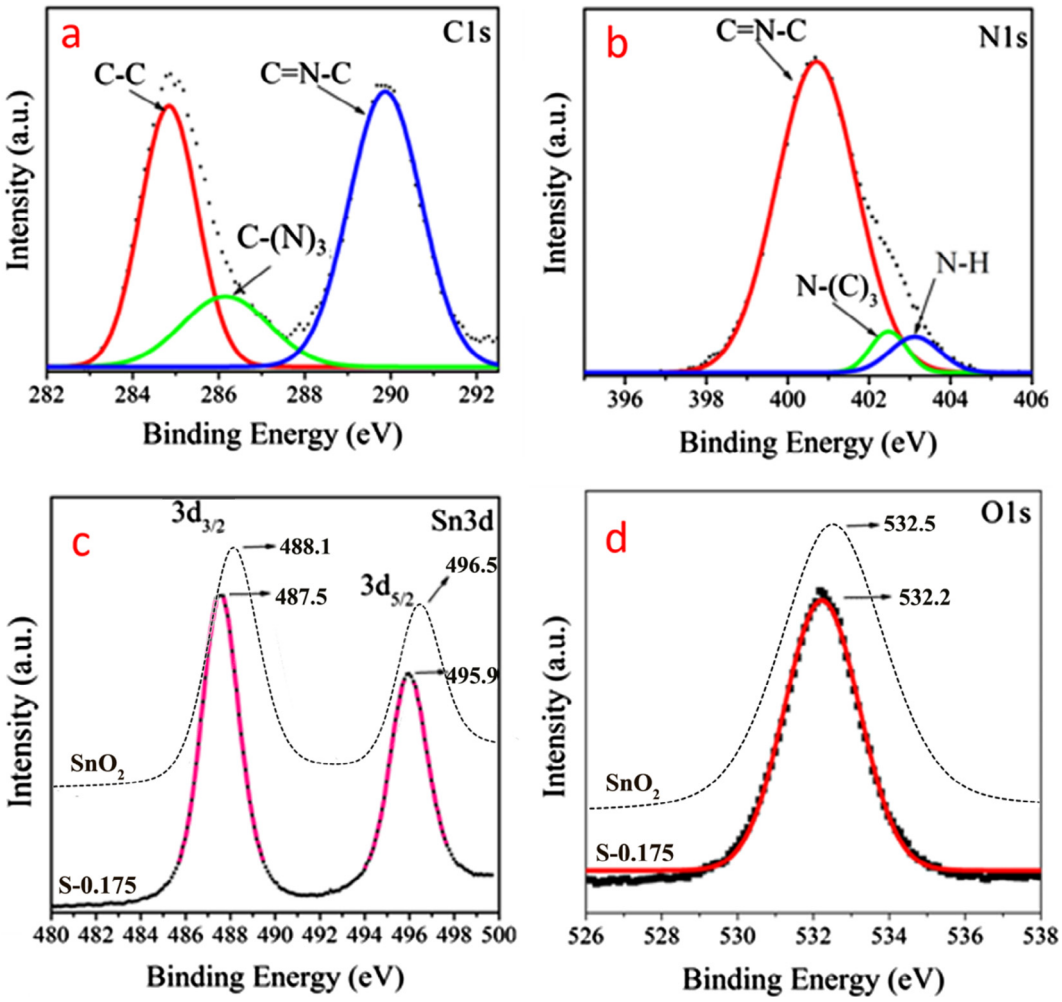

Fig. 6. High-resolution X-ray photoelectron spectrums of pure SnO_2 and S-0.175 samples: (a) C 1s spectrum, (b) N 1s spectrum, (c) Sn 3d spectrum, and (d) O 1S spectrum.

To determine how prepared sample is potentially beneficial for water-splitting reaction, the obtained electrode is analyzed in a linear sweep voltammetry (LSV) approach and recorded anodic currents are presented in Fig. 9. As can be seen, in the absence of light source, a negligible but nearly constant anodic current is measured which is enhanced significantly by lightening the electrode surface. The obtained photocurrent is slightly increased from 42 to 56 μA cm^{-2} when applied bias is anodically swept from −0.3 to +1.2 V due to facilitating charge transfer on the surface to initiate the water oxidation reaction.

To probe stability and sensitivity of the samples over the time, their photocurrent is measured versus time at a fixed +0.5 V applied bias which is shown in Fig. 10. The results illustrate that except first chopping cycle in which photo-response is decayed due to surface equilibration, it remained unchanged for the next illuminating intervals representing that the synthesized nanocomposites are durable photoactive materials for hydrogen production. Furthermore, it can be seen that the sample S-0.175 presented the highest photocurrent value as compared with the g-C_3N_4 sample and S-0.6 nanocomposite. Photo-response of the photo-anode reduced from 33 μA cm^{-2} for S-0.175 to 14 μA cm^{-2} for the sample S-0.6. This behavior is due to the reduction of the effective surface area of the photo-anode in the higher initial contents of tin, which is also confirmed by other analyses.

It is known that tin oxide is a semiconductor with wide band gap which is not photoactive in the visible range. However, this material in the nanoscale structure improves photoactivity of graphitic carbon nitride due to preventing the restacking of C_3N_4 nanosheets and enhancing the effective surface area. Another important role of the nano-sized tin oxide is creating suitable band bending to promote charge separation at the interface with g-C_3N_4 (through the formation of heterojunction) which enhances photocurrent as confirmed in the literature by a variety of analysis like photovoltage spectroscopy, photoluminescence measurements, and electrochemical impedance spectroscopy [17–19]. It should be mentioned that the existence of morphological defects such as pores can lead to the photoactivity improvement [33]. By preparing highly porous carbon nitride sheets, enhanced photoabsorption and improved charge carrier separation efficiency can be obtained [34].

The ability of photocatalytic degradation of a model dye under simulated visible light is also assessed for the nanocomposites and compared with that of the pure samples. The photocatalytic degradation efficiency is measured after 3 h illumination and the results are documented in Table 1. Although pure g-C_3N_4 could show considerable photocatalytic properties, pure SnO_2 is unable to degrade the dye under visible light irradiation. So, the formation of a heterojunction structure with a suitable ratio of the constituents and well dispersion of the nanoparticles on C_3N_4 sheets is necessary for their composites to reach a high photoactivity [13]. Here, g-C_3N_4/SnO_2 nanocomposite with the g-C_3N_4 mass ratio of 12.3% shows the highest photocatalytic activity, but by comparing with

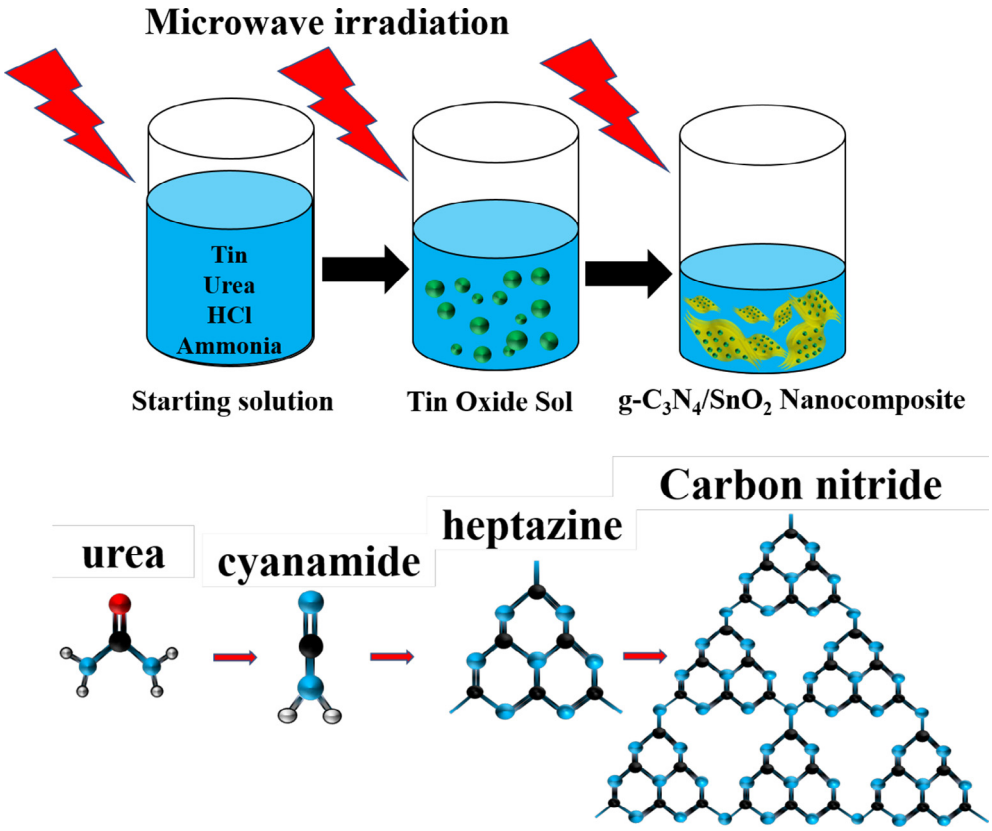

Fig. 7. The schematic pattern of carbon nitride synthesized via the microwave irradiation and urea pyrolysis in the presence of tin derivatives.

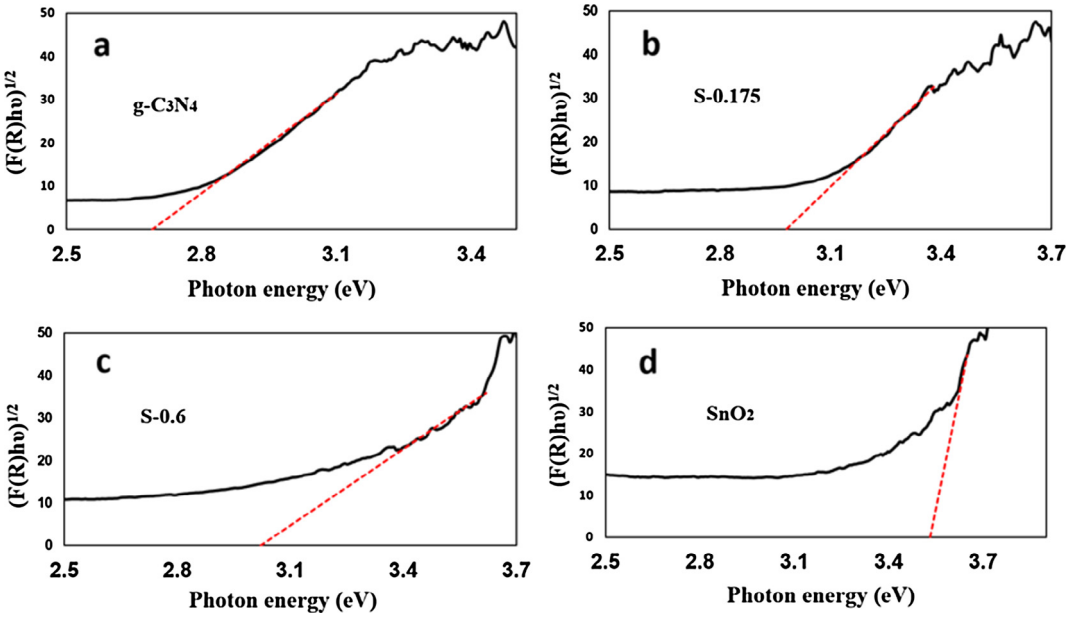

Fig. 8. The plot of $(F(R)h\upsilon)^{1/2}$ versus photon energy ($h\upsilon$) for the bandgap energy of pure samples and their nanocomposites.

the pure g-C_3N_4 sample, significant improvement in degradation of methylene blue has not been obtained. It should be noted that in order to compare the photocatalytic ability, we should consider both the degradation efficiencies and the amount of carbon nitride mass percentages that exists as the visible light photocatalysts. For this research, the S-0.175 sample contains only small amount of carbon nitride (12.3%) with the degradation efficiencies of higher than that of pure g-C_3N_4 sample So, the function of SnO_2 incorporation into the composite sample can be understood at this point and the synthesized nanocomposite shows a promising photocatalytic activity in addition to its high ability for solar water-splitting.

Photoluminescence (PL) spectra of pure g-C_3N_4, pure SnO_2, and S-0.175 nanocomposite are presented in Fig. 11 in order to

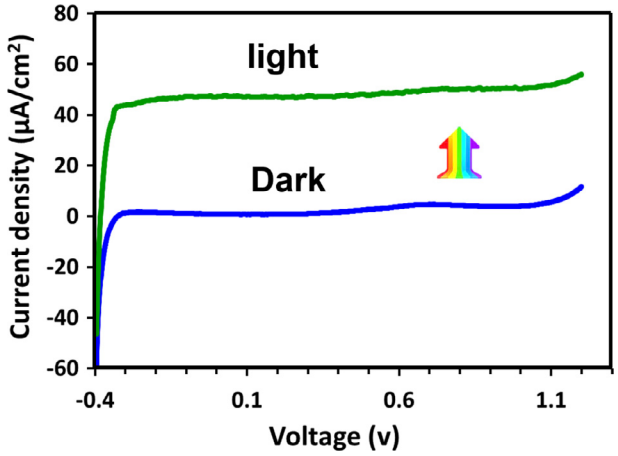

Fig. 9. LSV plot of the sample S-0.175 under dark and light conditions with the scan rate of 100 mV s^{-1}.

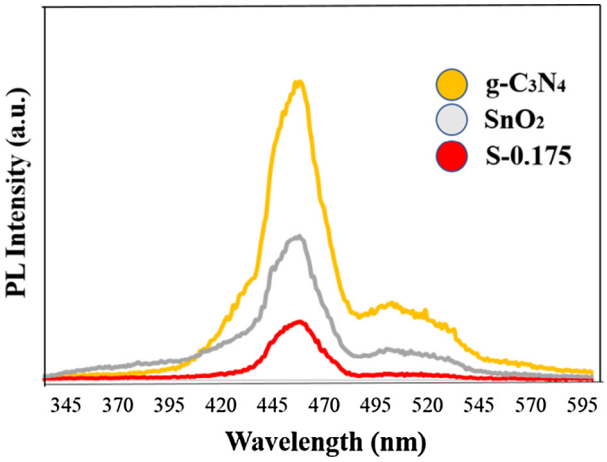

Fig. 11. PL spectra of pure g-C_3N_4, pure SnO_2, and their nanocomposite with the initial tin content of 0.175 g.

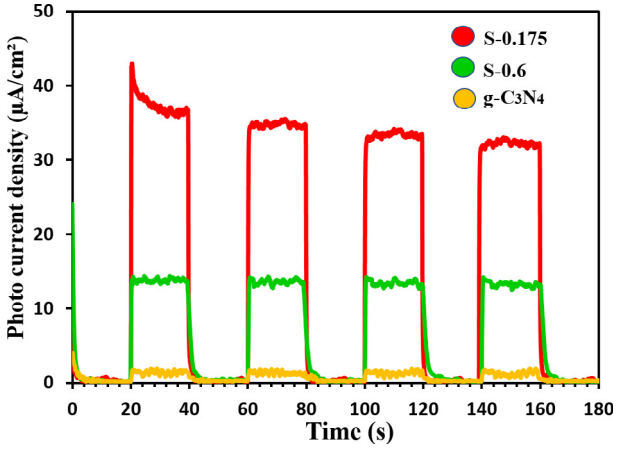

Fig. 10. Photocurrent versus time under a chopped condition at a constant applied bias of +0.5 V.

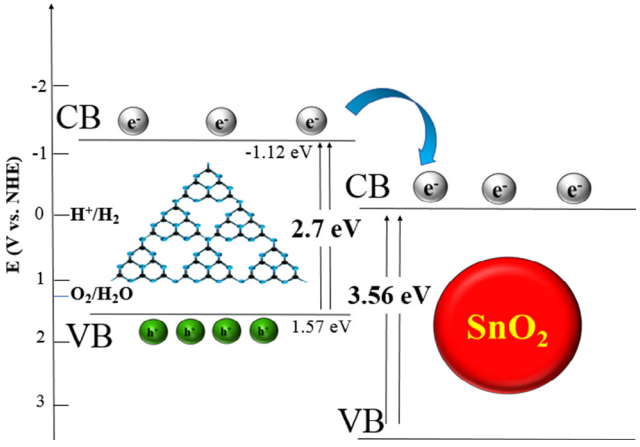

Fig. 12. Schematic illustration of g-C_3N_4/SnO_2 heterojunction under visible light irradiation.

investigate the electron-hole recombination properties of the samples. It is observed that the S-0.175 nanocomposite have the lowest PL Intensity among the other samples. This phenomenon indicates the better charge transfer ability of the prepared nanocomposite in comparison with that of the pure samples, suggesting that a heterojunction structure is formed. According to the Fig. 12, conduction band edge of g-C_3N_4 is more negative than that of tin oxide and because of that, the photogenerated electrons can be injected into the conduction band of SnO_2 (with regard to the interfacial contacts between the g-C_3N_4 and SnO_2 nanoparticles). Moreover, the valance bond of g-C_3N_4 is located between the CB and VB edges of Tin Oxide. So, with regard to the synthesized hybrid structure, formation of staggered gap (type II) heterojunction with the ability of solar water splitting could be indicated.

4. Conclusions

In the present study, microwave irradiation was utilized for the first time in order to synthesize g-C_3N_4/SnO_2 nanocomposites by simple pyrolysis of urea with the aid of SnO_2 nanoparticles. The creation of surface OH groups in the form of Sn-OH-Sn bridges during the hydrolysis and condensation of tin precursor were shown to be responsible for the effective conversion of urea to carbon nitride sheets. Ultra-small SnO_2 nanoparticles were in-situ synthesized and intercalated into the porous layers of g-C_3N_4, preventing their restacking. The carbon nitride sheets were attached to the aggregates of SnO_2 nanoparticles mainly through hydrogen bonds. This could result in the formation of a heterojunction structure with potential enhancement in charge transfer and charge

Table 1
Summary of physicochemical characteristics of the samples in the present study.

Sample name	S_{BET} (m^2 g^{-1})	Crystallite size (nm)	Band gap (eV)	I_{ph} (μA cm^{-2})	Photocatalytic degradation efficiency (%)
g-C_3N_4	17	–	2.7	–	40.8 ± 11
S-0.175	195	6.8 ± 2.3	2.98	33	41.2 ± 4.1
S-0.6	79	10.3 ± 2.7	3.02	14	21.3 ± 0.7
S-1	3	–	–	–	–
SnO_2	101	7.0 ± 1.4	3.53	3	4.9 ± 1.4

separation time together with the high effective surface area. It was of great interest that by using urea as a low-cost precursor of carbon nitride and through the simple and fast preparation route of microwave-assisted synthesis, a nanocomposite of g-C_3N_4/SnO_2 was obtained with enhanced photocatalytic activity in the visible light region. The nanocomposite represented a stable photocurrent density of 33 μA cm^{-2} over several cycles and it can be introduced as an efficient water-splitting catalyst and a high-performance candidate for clean energy production.

Acknowledgement

The authors would like to express their sincere appreciation to Prof. Madaah Hosseini for his valuable assistance. Special thanks go to Mrs. Rouhani and Mr. Charkhesht who were the expert assistants to reach some of the goals in the present work. The authors acknowledge the facilities, and the scientific and technical assistance, of the Australian Microscopy & Microanalysis Research Facility at RMIT University. General support of the Iran National Science Foundation and the Iran Nanotechnology Initiative Council (INIC) is acknowledged.

References

[1] Y. Wang, X. Wang, M. Antonietti, Polymeric graphitic carbon nitride as a heterogeneous organocatalyst: from photochemistry to multipurpose catalysis to multipurpose catalysis to sustainable chemistry, Angew. Chem. Int. Ed. 51 (2012) 68–89.
[2] H. Li, F. Zhao, J. Zhang, L. Luo, X. Xiao, Y. Huang, H. Ji, Y. Tong, A g-C_3N_4/WO_3 photoanode with exceptional ability for photoelectrochemical water-splitting, Mater. Chem. Front. 1 (2017) 338–342.
[3] Y. Dong, Y. Chen, P. Jiang, G. Wang, X. Wu, R. Wu, A novel g-C_3N_4 based photocathode for photoelectrochemical hydrogen evolution, RSC Adv. 6 (2016) 7465–7473.
[4] M.M. Khan, S.A. Ansari, D. Pradhan, M.O. Ansari, D.H. Han, J. Lee, M.H. Cho, Band gap engineered TiO_2 nanoparticles for visible light induced photoelectrochemical and photocatalytic studies, J. Mater. Chem. A 2 (2014) 637–644.
[5] R.C. Pawar, V. Khare, C.S. Lee, Hybrid photocatalysts using graphitic carbon nitride/cadmium sulfide/reduced graphene oxide (g-C_3N_4/CdS/RGO) for superior photodegradation of organic pollutants under UV and visible light, Dalt. Trans. 43 (2014) 12514–12527.
[6] S. Li, G. Dong, R. Hailili, L. Yang, Y. Li, F. Wang, Y. Zeng, C. Wang, Effective photocatalytic H_2O_2 production under visible light irradiation at g-C_3N_4 modulated by carbon vacancies, Appl. Catal. B: Environ. 190 (2016) 26–35.
[7] L.S. Lin, Z.X. Cong, J. Li, K.M. Ke, S.S. Guo, H.H. Yang, G.N. Chen, Graphitic-phase C_3N_4 nanosheets as efficient photosensitizers and pH-responsive drug nanocarriers for cancer imaging and therapy, J. Mater. Chem. B 2 (2014) 1031–1037.
[8] X. Zhuang, Y. Mai, D. Wu, F. Zhang, X. Feng, Two-dimensional soft nanomaterials: a fascinating world of materials, Adv. Mater. 27 (2015) 403–427.
[9] S. Martha, A. Nashim, K.M. Parida, Facile synthesis of highly active g-C_3N_4 for efficient hydrogen production under visible light, J. Mater. Chem. A 1 (2013) 7816–7824.
[10] S.C. Yan, Z.S. Li, Z.G. Zou, Photodegradation performance of g-C_3N_4 fabricated by directly heating melamine, Langmuir 25 (2009) 10397–10401.
[11] H.B. Fang, Y. Luo, Y.Z. Zheng, W. Ma, X. Tao, Facile large-scale synthesis of urea-derived porous graphitic carbon nitride with extraordinary visible-light spectrum photodegradation, Ind. Eng. Chem. Res. 55 (2016) 4506–4514.
[12] L. Shi, L. Liang, F. Wang, M. Liu, K. Chen, K. Sun, N. Zhang, J. Sun, Higher yield urea-derived polymeric graphitic carbon nitride with mesoporous structure and superior visible-light-responsive activity, ACS Sustain. Chem. Eng. 3 (2015) 3412–3419.
[13] X.J. Wang, W.Y. Yang, F.T. Li, Y.B. Xue, R.H. Liu, Y.J. Hao, In situ microwave-assisted synthesis of porous N-TiO_2/g-C_3N_4 heterojunctions with enhanced visible-light photocatalytic properties, Ind. Eng. Chem. Res. 52 (2013) 17140–17150.
[14] G. Dong, Y. Zhang, Q. Pan, J. Qiu, A fantastic graphitic carbon nitride (g-C_3N_4) material: electronic structure, photocatalytic and photoelectronic properties, J. Photochem. Photobiol. C Photochem. Rev. 20 (2014) 33–50.
[15] V. Vo, X.D. Nguyen Thi, Y.S. Jin, G.L. Thi, T.T. Nguyen, T.Q. Duong, S.J. Kim, SnO_2 nanosheets/g-C_3N_4 composite with improved lithium storage capabilities, Chem. Phys. Lett. 674 (2017) 42–47.
[16] H. Shen, X. Zhao, L. Duan, R. Liu, H. Li, Enhanced visible light photocatalytic activity in SnO_2@g-C_3N_4 core-shell structures, Mater. Sci. Eng. B 218 (2017) 23–30.
[17] F. Raziq, Y. Qu, M. Humayun, A. Zada, H. Yu, L. Jing, Synthesis of SnO_2 /B-P codoped g-C_3N_4 nanocomposites as efficient cocatalyst-free visible-light photocatalysts for CO_2 conversion and pollutant degradation, Appl. Catal. B: Environ. 201 (2017) 486–494.
[18] Y. He, L. Zhang, M. Fan, X. Wang, M.L. Walbridge, Q. Nong, Y. Wu, L. Zhao, Z-scheme SnO_{2-x}/g-C_3N_4 composite as an efficient photocatalyst for dye degradation and photocatalytic CO_2 reduction, Sol. Energy Mater. Sol. Cell. 137 (2015) 175–184.
[19] Ch. Fettkenhauer, G. Clavel, K. Kailasam, M. Antonietti, D. Dontsova, Facile synthesis of new, highly efficient SnO_2/carbon nitride composite photocatalysts for the hydrogen evolution reaction, Green Chem. 17 (2015) 3350–3361.
[20] M.R. Mohammadi, R.R.M. Louca, D.J. Fray, M.E. Welland, Dye-sensitized solar cells based on a single layer deposition of TiO_2 from a new formulation paste and their photovoltaic performance, Sol. Energy 86 (2012) 2654–2664.
[21] X. Chen, B. Zhou, S. Yang, H. Wu, Y. Wu, L. Wu, J. Pan, X. Xiong, In situ construction of an SnO_2/g-C_3N_4 heterojunction for enhanced visible-light photocatalytic activity, RSC Adv. 5 (2015) 68953–68963.
[22] Y. Zang, L. Li, X. Li, R. Lin, G. Li, Synergistic collaboration of g-C_3N_4/SnO_2 composites for enhanced visible-light photocatalytic activity, Chem. Eng. J. 246 (2014) 277–286.
[23] X. Liu, N. Chen, Y. Li, D. Deng, X. Xing, Y. Wang, A general nonaqueous sol-gel route to g-C_3N_4-coupling photocatalysts: the case of Z-scheme g-C_3N_4/TiO_2 with enhanced photodegradation toward RhB under visible-light, Sci. Rep. 6 (2016) 39531–39546.
[24] S. Ding, X. Wen (David) Lou, SnO_2 nanosheet hollow spheres with improved lithium storage capabilities, Nanoscale 3 (2011) 3586–3588.
[25] J. Tang, J. Yang, L. Zhou, J. Xie, G. Chen, X. Zhou, Layer-by-layer self-assembly of a sandwich-like graphene wrapped SnO_x@graphene composite as an anode material for lithium ion batteries, J. Mater. Chem. A. 2 (2014) 6292–6295.
[26] F. Soleimani, H.R. Madaah Hosseini, F. Ordikhani, M. Mokhtari-Dizaji, Enhancing sonocatalytic properties of TiO_2 nanocatalysts by controlling the surface conditions: effect of particle size and PVA modification, Desalin. Water Treat. 57 (2016) 28378–28385.
[27] Y. Zhang, J. Liu, G. Wu, W. Chen, Porous graphitic carbon nitride synthesized *via* direct polymerization of urea for efficient sunlight-driven photocatalytic hydrogen production, Nanoscale 4 (2012) 5300–5303.
[28] Y. Liu, M. Qin, L. Zhang, B. Jia, Z. Cao, D. Zhang, X. Qu, Solution combustion synthesis of Ni–Y_2O_3 nanocomposite powder, Trans. Nonferr. Met. Soc. China 25 (2015) 129–136.
[29] S. Zhang, J. Yan, S. Yang, Y. Xu, X. Cai, X. Li, X. Zhang, Electrodeposition of Cu_2O/g-C_3N_4 heterojunction film on an FTO substrate for enhancing visible light photoelectrochemical water-splitting, Chin. J. Catal. 38 (2017) 365–371.
[30] J. Cao, C. Qin, Y. Wang, H. Zhang, B. Zhang, Y. Gong, X. Wang, G. Sun, H. Bala, Z. Zhang, Synthesis of g-C_3N_4 nanosheet modified SnO_2 composites with improved performance for ethanol gas sensing, RSC Adv. 7 (2017) 25504–25511.
[31] X.X. Zou, G.D. Li, Y.N. Wang, J. Zhao, C. Yan, M.Y. Guo, L. Li, J.S. Chen, Direct conversion of urea into graphitic carbon nitride over mesoporous TiO_2 spheres under mild condition, Chem. Commun. 47 (2011) 1066–1068.
[32] C.J. Cornelius, E. Marand, Hybrid inorganic-organic materials based on a 6FDA-6FpDA-DABA polyimide and silica: physical characterization studies, Polymer 43 (2002) 2385–2400.
[33] Z. Zhang, Y. Zhang, L. Lu, Y. Si, S. Zhang, Y. Chen, K. Dai, P. Duan, L. Duan, J. Liu, Graphitic carbon nitride nanosheet for photocatalytic hydrogen production: the impact of morphology and element composition, Appl. Surf. Sci. 391 (2017) 369–375.
[34] L. Luo, A. Zhang, M.J. Janik, K. Li, C. Song, X. Guo, Facile fabrication of ordered mesoporous graphitic carbon nitride for RhB photocatalytic degradation, Appl. Surf. Sci. 396 (2017) 78–84.